Article:
Hanson, BS orcid.org/0000-0002-6079-4506 and Dougan, L orcid.org/0000-0002-2620-5827 (2020) Network Growth and Structural Characteristics of Globular Protein Hydrogels. Macromolecules, 53 (17). pp. 7335-7345. ISSN 0024-9297

https://doi.org/10.1021/acs.macromol.0c00890

Network Growth and Structural Characteristics of Globular Protein Hydrogels

Benjamin S. Hanson*,† and Lorna Dougan*,†,‡

†*School of Physics and Astronomy, University of Leeds, Leeds, UK*

‡*Astbury Centre for Structural Molecular Biology, University of Leeds, Leeds, UK*

E-mail: b.s.hanson@leeds.ac.uk; l.dougan@leeds.ac.uk

Abstract

Folded protein-based hydrogels are a novel class of biomaterials which combine the useful viscoelastic properties of individual proteins together with the prospect of rational design principles. Whilst the macroscopic properties of these materials have been well-studied, there is a paucity of understanding of their mesoscopic formation mechanisms, especially given the differences in building block compared to biopolymer hydrogels.

We present the results of a simulation study into the growth of polymeric networks of chemically cross-linked folded proteins that form the structural backbone of these hydrogels, observing how experimentally controllable parameters affect the resultant network growth and structural characteristics. We show that the initial volume fraction emerges as the dominant parameter at the network level, but that the properties of the single protein remain important. We ultimately show that we can tune the properties of a monodisperse protein hydrogel network only within limits which are dictated primarily by implicit diffusion time scales.

Introduction

In recent years there has been a push throughout the life sciences, soft matter sciences and bio/nano-sciences to design so-called 'smart' biomaterials. This somewhat umbrella terminology refers to a general class of idealised materials which would respond in some way to either external physical or chemical stimuli, or directly to human intervention, and subsequently alter their behaviour in such a way as to optimise their performance in their designed task. Amongst these materials are biological hydrogels,[1–3] which are usually formed when some type of hydrophilic biopolymer is induced into forming a cross-linked, percolating network.[4,5] The hydrophilicity of the network draws in relatively large quantities of water and causes significant expansion, whereas the subsequent elastic response of the network (whether entropic or enthalpic in origin) counters the expansion. The result is a stable, viscoelastic equilibrium state; a hydrogel.[6,7]

Due to the high water content[8,9] and the underlying components from which they are formed, these objects are often intrinsically biocompatible and therefore have a diverse array of biomedical applications.[10–16] Due to their structural and mechanical similarity to the extra-cellular matrix environment, the clinical applications of hydrogels often focus on mimicking this either internal to the body, such as for tissue engineering or drug delivery[14,16–18] or external to the body, such as for wound healing.[19–21] Proteins, then, as the functional units of the body, are also an attractive structural subunit if one wishes to develop a diverse class of smart materials within an ECM-like environment. Proteins have unique nanoscale viscoelastic properties in that they can elastically deform up to a certain point with an enthalpic response from the intra-protein bonds, but once these bonds break, the protein will begin to unfold and respond entropically as an amino-acid chain.[22] Nevertheless, both prior to and following unfolding, connected proteins (whether by cross-links or amino-acid chains) exhibit a polymeric response akin to standard biopolymers.[23] Additionally, folded proteins have inherent biological functionality that, if preserved within the hydrogel network, may be exploited in a controlled fashion. Although some clinical applications have

been suggested,[24,25] significantly less is known about the generalised behaviour of protein hydrogels.

Wu *et al.* showed that the qualitative properties of the protein building blocks (ductility, toughness, stiffness etc) can be translated to the macroscale,[26] indicating that rational design is possible. Recently, using maltose binding protein (MBP) as the protein building block, Hughes *et al.* were able to show that the intrinsic functionality of the individual proteins can also be exploited as a part of this rational design process.[27] By measuring the multi-scale structural characteristics of MBP hydrogels in the presence of varying amounts of maltose, they were able to show, using a variety of experimental techniques, that not only do most of the proteins still exist in their folded state within the swelled network, but that mechanically strengthening those proteins via binding maltose strengthens the overall hydrogel. They also provide a novel structural justification for these observations. Earlier experiments by Da Silva *et al.* further showed that the effect of having intermediate structure in the form of small polyproteins also translates to the macroscale,[28] and bespoke simulations by Shmilovich and Popa confirm this,[8] going so far as to suggest that macroscopic behaviour could be used to infer ensemble protein unfolding kinetics. Indeed, recent work has suggested that it is the protein unfolding itself that leads to the emergent viscoelastic behaviour measured in protein hydrogels.[27,29,30] For those interested in the full scope of research in this area, a comprehensive review by Li *et al.* [1] was recently published.

Importantly for this work, Grad *et al.* were recently able to design highly specific network building blocks to show that in addition to the cross-linking kinetics, the network topology of a hydrogel affects its stress relaxation capabilities.[31] Whilst Grad *et al.* used intermediate coiled-coils as cross-links between polymer chains, other methods of cross-linking are available such as direct covalent cross-links or physical interactions.[32,33] Nevertheless, their work implies that microscopic connectivity limits on cross-linking can also translate to the macroscale. Correspondingly, at the single protein level there are a variety of experimental techniques that can be employed to engineer the specific properties of the protein building

blocks used to form these types of protein-based hydrogel.[22,34,35] By choosing a base protein sequence and using standard E.coli expression methods,[34] we can effectively choose an initial size, shape and mechanical type of building block.[36] Protein engineering around this base structure allows us to design specific residues which, if exposed to light, will radicalise, thus making them candidates for covalent chemical cross-linking.[1] Ruthenium catalysed cross-linking techniques[37] are currently used in our group,[27] where (primarily) surface-accessible tyrosine residues are made able to form covalent bonds with one another on exposure to light, but as with standard polymer hydrogels, other methods are available[32,33] and may be sometimes be required.[38] Whichever the case, if these cross-links are sparse enough, such alterations ought not to affect the secondary and tertiary structures of the proteins, giving us two nanoscale variables to alter when designing folded protein-based hydrogels: the single-protein binding site distribution, and the size of the protein itself. Together with the overall protein concentration / volume fraction, we have a rich, controllable parameter space with which to alter the physical properties of folded protein-based hydrogels.

Currently missing from the wealth of research is a detailed structural and mechanical understanding of these systems spanning the biological mesoscale. It has been previously noted that whilst we can characterise the macroscopic properties of ECM mimicking materials, it is difficult to predict what these properties will be given knowledge of only the singular component structures.[39] With standard polymer hydrogels, in fact, the 'fundamental unit', as we might define by the average pore size or amount of polymer between cross-links, remains almost unknown until the hydrogel has formed. Whilst sophisticated models exist which can model this swelling behaviour, they are often general, mathematically continuous models which therefore do not explicitly refer to underlying structure, and can be empirically parameterised for almost any system.[40,41] With globular protein hydrogels on the other hand, our fundamental unit must be the single globular protein, which can be engineered to have a specific properties and is what subsequently unfolds upon swelling. For developing rational design principles for protein hydrogels, then, it is necessary to investigate how these

nanoscale properties translate to the macroscale. For example, whilst we may be able to infer a relationship between the system-wide cross-linking density and macroscopic properties of protein hydrogels, it is not yet clear how these densities emerge as a function of the individual protein structure. Similarly, whilst we are starting to see that protein unfolding can contribute towards mediating the elastic response throughout the hydrogel network,[30] is not yet clear which proteins unfold and why.[42] Given that we have experimental control over the single protein structure, these questions are vital in terms of rational design.

Here, we present our initial investigation into the formation mechanisms of folded protein-based hydrogels and the subsequent hierarchical emergence of their mesoscopic properties. Using bespoke coarse-grained mesoscale simulations, we observe how the specific size of the individual monomeric protein subunits and the number of cross-link sites on each, together with their overall concentration, affects the growth dynamics and resulting structural properties of folded protein-based hydrogels, prior to the onset of swelling and subsequent protein unfolding. We then discuss how these structural characteristics will likely affect the distribution of force throughout the network and the resultant mechanical behaviour as the hydrogel begins to swell.

Methods

BioNet - A Dynamic Simulation Model

To analyse the formation of folded protein-based hydrogel networks we utilised BioNet, a simulation platform currently under development in our group. BioNet models a set of N interacting proteins, each as an independent, spherical object with radius R. It also models explicit connections between the proteins (in our case, covalent chemical cross-links) as Hookean springs with spring constant k_{cl} and equilibrium length l_{cl}. These objects are simulated using a Brownian dynamics approach, where each sphere has an associated isotropic drag $\lambda = 6\pi\mu R$ dependent upon the local background viscosity μ, and is subject to thermal

noise consistent with the fluctuation-dissipation theorem.

As detailed in our previous work,[23] BioNet objects have real, three-dimensional physical structure and thus, the defined chemical cross-links connect proteins to one another at point-like binding sites defined explicitly at the surface. Together with a soft-core steric potential, this enables stiffness and percolation to hierarchically emerge as a function of the network connectivity and individual subunit properties as the simulation progresses. This steric potential, U_s, is of the form

$$U_s = \frac{1}{2} k_s \left(\frac{V_o}{A_{cs}} \right)^2, \tag{1}$$

where V_o is the volume overlap between two spheres, A_{cs} is the cross-sectional area of each sphere and hence, k_s is a linear stiffness constant with units comparable to a Hookean spring. However, because the potential is a function of the *volume* overlap, then U_s scales with r^6, where r is the distance between two spheres, and with R^6. Hence, Eq. 1 allows us to implicitly, but efficiently, capture the effects of intrinsic stiffness and volumetric deformation. The parameters used in our simulation are given in Table 1.

As the binding sites are located explicitly at the surface of each protein, their local geometric organisation on the surface of the protein is a parameter of importance. Therefore, in addition to translational degrees of freedom, we include the rotational motion of each sphere within our BioNet model, with associated rotational drag and thermal noise included.[43]

As these simulations are primarily investigating the initial formation and structural characteristics of the underlying networks of protein hydrogels, and not their mechanical response, we have explicitly chosen not to include protein unfolding at this stage. Nevertheless, our study provides evidence of the formation mechanisms which may lead to the distribution of protein unfolding within a hydrogel network and will be the topic of future research.

Simulating Chemical Cross-linking

Within BioNet simulations, if cross-linking is enabled, then if two binding sites on two different proteins come within a distance of $2l_{cl}$ of one another and are not already bonded, then a bond will form between them. These bonds are not perfectly representative of a real carbon-carbon bond as the true stiffness of these bonds would severely limit our numerical integration timestep.[44] Instead, we set the stiffness by letting the fluctuations about the equilibrium length of this bond to be a factor of ten lower than the smallest radius used, and therefore effectively negligible. We also assume that the energy well is so deep in these bonds that, once formed, they cannot break. Whilst BioNet is also capable of introducing a cross-linking reaction rate, such that each binding site has a probability of being 'active' or not, we have not investigated that parameter in these simulations. Hence, our simulations can be assumed to be within the regime of diffusion-limited aggregation.[45] Nevertheless, the explicit positioning of cross-links on the surface of each protein enables real three-dimensional percolating networks to form, with structure determined by the specific cross-links that form and with rigidity determined by some combination of the protein-protein bonds and the soft-core steric potential.[23]

Simulation Suite and Protocols

Our simulations consist of a parameter sweep over a variety of different protein volume fractions, f_v, protein cross-linking / binding site topologies, which are labelled simply by the number of sites per protein, N_s, and two protein sizes represented by their radius R. Table 1 gives the specific values used, and Figure 1 shows the structures of each of the protein monomers.

We chose our protein radii to represent some of the specific systems being considered in our group,[27] whereas the values of N_s were chosen to give a range of rotational symmetries for each subunit. Finally, the volume fractions were chosen to cover much of the range of existing experimental work throughout the literature concerning globular pro-

Table 1: Left: The physical simulation parameters used that are constant across all simulations. Right: The range of variable parameters investigated in this work.

Constant Parameter	Value	Variable Parameter	Values
Number of proteins, N	10000	Sites per protein, N_s	4,6,8,14
Steric elastic constant, k_s	1560 pN.nm	Volume fraction, f_v	0.5%, 1%, 5%, 7%, 10%
Cross-link elastic constant k_{cl}	411 pN.nm	Protein radius, R	1nm,2.5nm
Cross-link equilibrium length, l_{cl}	0.15 nm		
Background viscosity, μ	0.001 Pa.s		

tein hydrogels.[1,8,9,26,29,30,46–49] It has been noted that many experiments involving globular protein hydrogels are performed at relatively high volume fractions, often close to the solubility limit.[26,46] Assuming a protein density of 1.35g/cm^3 [50] and taking the value of 100mg/ml quoted by Wu *et al.* ,[26] then protein hydrogels are usually experimentally formed at $f_v >\sim 0.07$. With an approximate lower limit for the minimum gelation concentration for bovine serum albumin (BSA) hydrogels of 0.7mM[9] ($f_v \sim 0.01$), we wanted to both cover this range, and observe the potential causes of this inability to form a gel at low f_v as part of this investigation.

For each of the possible combinations of variable parameters in Table 1, we performed three independent simulations for statistical analysis. Due to the potential dependence on the initial state of the subsequent network that forms for diffusion-limited aggregating systems, rigorous thermodynamically consistent randomisation of the initial state was performed, as detailed in the Supplementary Information. All results shown have been averaged over these three repeats, with standard errors calculated by assuming normally distributed variations between repeats. To achieve numerical stability and accuracy in the simulations, our numerical integration timestep dt was set to be a factor of ten lower than the fastest estimated time scale within the system. We assumed this to be the relaxation of the permanent chemical cross-links due to them being the most rigid mechanical objects in the system. Hence, $dt = 4.59$ps.

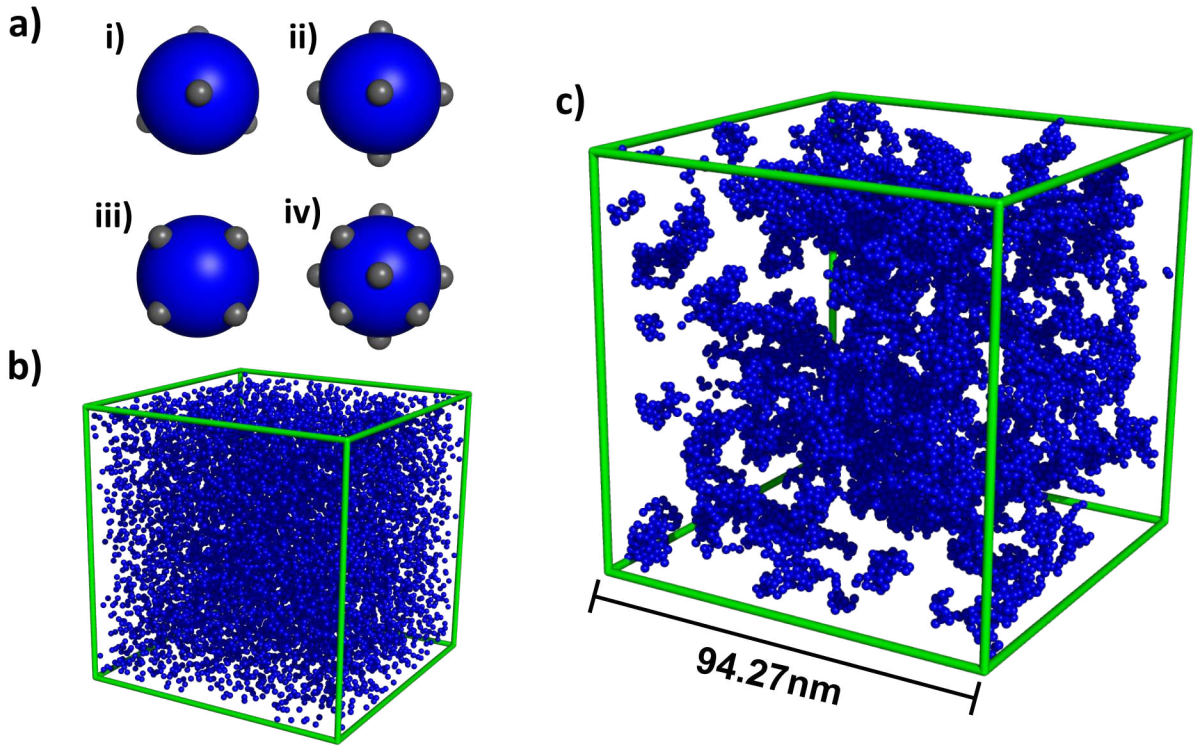

Figure 1: The structural components used and subsequent formation of a protein hydrogel network within a BioNet simulation. **a)** The four types of building block (blue spheres) used, defined by the different cross-link site topologies (smaller grey spheres). i) $N_s = 4$, sites in a tetrahedral arrangement. ii) $N_s = 6$, sites in a cubic (face-centered) arrangement. iii) $N_s = 8$, sites in a cubic (corners) arrangement. iv) $N_s = 14$, a combination of the $N_s = 6$ and $N_s = 8$ topologies. **b)** A representative structure of a mechanically relaxed initial state of a BioNet simulation before cross-linking is initiated. **c)** The final state of a simulation performed with $N_s = 8$ cross-link sites, volume fraction $f_v = 0.05$ and protein radius $R = 1$nm. Movies showing the evolution of network formation are provided as Supplementary Information.

Results

Network Growth

The emergence of network coordination and spatial cross-link density

In standard biopolymer networks and hydrogels, the density of cross-links is related to the resultant network elasticity.[51] We therefore begin our analysis by calculating the evolution of both the average number of cross-links formed on each protein (the cross-link coordination number), C_{cl}, and the average spatial cross-link number density, n_{cl}. Whilst these values are directly related, differing only by a scaling factor, their individual interpretations with respect to the overall hierarchical structural organisation is of vital importance.

Visual inspection of the simulations show that intermediate clusters form, which continue to join until percolation is reached. We define a cluster as a mathematical network of nodes and connections, such that two proteins are in the same cluster if they are connected in some way by intermediate bonds and proteins. Thus, our definition of clusters has little to do with how these objects geometrically pack in physical space, only by how they are connected by mechanical components. Percolation was measured using a form of cluster analysis,[52] as detailed in the Supplementary Information.

Figure 2 shows the evolution of C_{cl} over the course of a simulation at each of the values of N_s, for two different values of f_v and with $R = 2.5$nm. We can see that an increase in f_v appears to increase the rate at which C_{cl} grows over the course of a simulation, whereas altering N_s radically alters the asymptotic value of the growth process. The n_{cl} traces, differing only by a scaling factor, show equivalent behaviour in this regard. We also note from Figure 2b that no matter the value of N_s, C_{cl} never reaches full saturation, showing that there are some cross-link sites within the system that remain unoccupied.

To investigate this trend explicitly, to each of the curves in Figure 2, and to the related n_{cl} curves, we fit an empirical function of the form

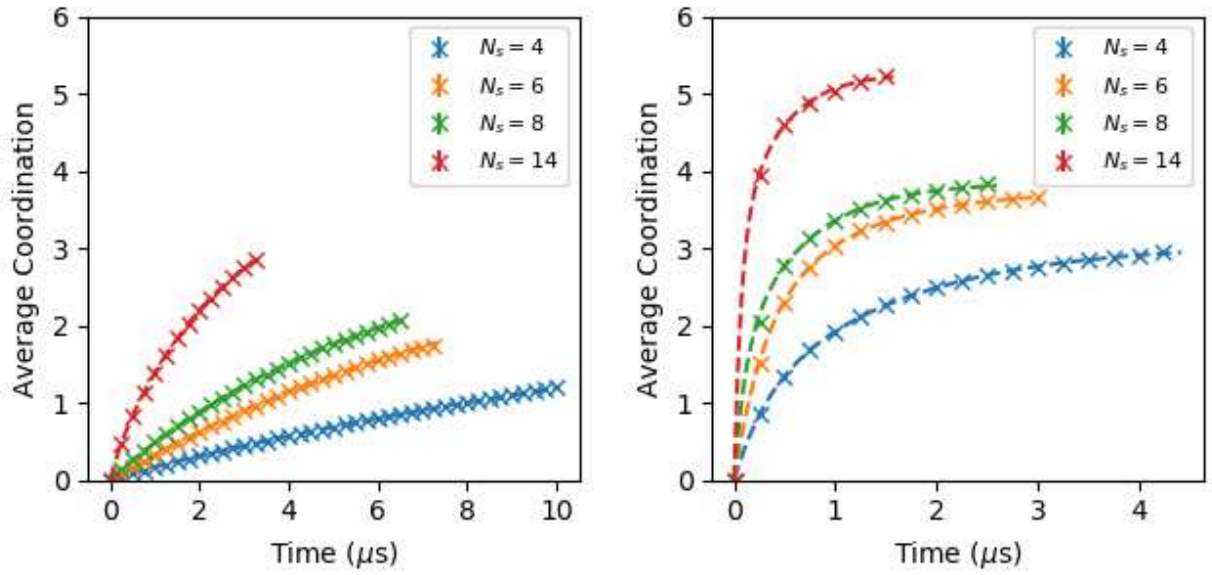

(a) (b)

Figure 2: The evolution of the average cross-link coordination number over the course of simulations formed of proteins with radius $R = 2.5$nm, shown for multiple cross-link site topologies, N_s, and two volume fractions, f_v. Each trace has an empirical fitting function overlaying the data. a) $f_v = 0.005$. b) $f_v = 0.1$.

$$y = \sum_{i=1}^{N_p} A_i \left(1 - \exp\left(-\frac{t}{\tau_i}\right)\right) \tag{2}$$

where each i corresponds to some decaying growth process with an as yet unknown cause, N_p is the minimum number of growth processes required to accurately characterise the data, and y corresponds to either C_{cl} or n_{cl}. We found in all cases for $N_p > 2$ that any additional parameters became indeterminate under a least-square fitting protocol, meaning that two distinct process can be resolved over these timescales. We hypothesise, based on the parameters in Eq. 2 extracted and detailed in the Supplementary Information, that these two time scales correspond to inter-cluster and intra-cluster cross-linking. Of most importance here though is the value $y_\infty = \sum_i A_i$, which corresponds to the extrapolated final value of y as $t \to \infty$. Figure 3 shows this value plotted as a function of f_v and N_s as applied to both the C_{cl} data and the associated n_v data.

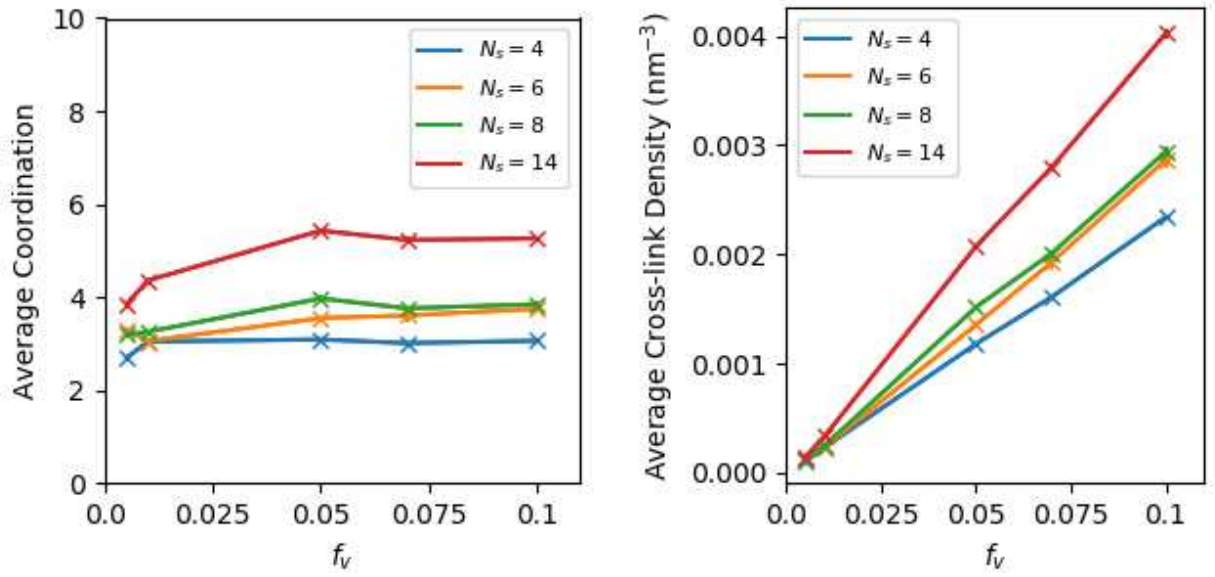

(a) (b)

Figure 3: The extrapolated value defining the expected final state of the network, and calculated through fitting Eq. 2 to the relevant data for $R = 2.5$nm simulations. a) Cross-link coordination number, C_{cl}. b) Spatial cross-link density, n_{cl}.

We now see clearly from Figure 3a that f_v has very little effect on the average cross-link coordination number except, apparently, at very low f_v. However, through inspection of these lower f_v simulations ($f_v = 0.005$ and $f_v = 0.01$), we actually observe that full percolation has not occurred in these systems and so it may be the case that application of Eq. 2 (to the curve in Figure 2a) will have underestimated the values defining a percolated network structure. Indeed as previously mentioned, a recent study by Khoury *et al.* suggested that systems with such a low volume fraction may not form a gel at all.[9] This is likely due to the fact that the clusters collapse much too quickly in comparison to the diffusion time between clusters, and thus cannot easily fill space. Nevertheless, we see that the number of available cross-link sites is the determining factor in the overall average cross-link coordination throughout the network. This qualitatively corresponds to experiments performed by Grad *et al.* [31] in that our monomers can also be microscopically designed to alter the network topology to some extent.

On the other hand, by scaling each of the values in Figure 3a by the corresponding spatial protein number density implicitly defined by f_v, we obtain Figure 3b. Now we see that whilst N_s determines the overall cross-link density *per network object* i.e. the cross-link coordination number, f_v alters the number of those objects distributed in physical space. We therefore see that both f_v and N_s have comparable effects on the overall cross-link density throughout physical space. Yet, that we can add additional proteins into the system (increase f_v) whilst keeping the average cross-link coordination constant suggests that we may also be keeping the overall network topology approximately constant, which is explored further in later sections.

The protein size affects both the cross-link coordination and spatial cross-link density via two distinct mechanisms

To investigate this interplay between cross-link coordination and spatial cross-link density further, we performed the same analysis on the $R = 1$nm simulation set. Given that we have the same relative diffusional dynamics, our initial assumption was that with all other parameters unchanged, a reduction in the physical separation between cross-links (on the same protein) would increase the overall spatial cross-link density whilst keeping the cross-link coordination per protein constant. The results of this analysis are shown in Figure 4.

We observe the same overall trends in the curves, in that f_v and N_s have the same qualitative dependences as in the $R = 2.5$nm simulations (albeit with faster relaxation, as detailed in the Supplementary Information). However, we can clearly see that in Figure 4a, each of the cross-link coordination values are higher than their equivalents in Figure 3a. We also note that for the $N_s = 14$ system, C_{cl} increases beyond six, which one might expect to be the maximum given geometric considerations. This phenomenon is due to the fact that for such small objects, where cross-link sites are relatively close to one another on the surface of each protein, multiple bonds have formed between the same two proteins (the specific

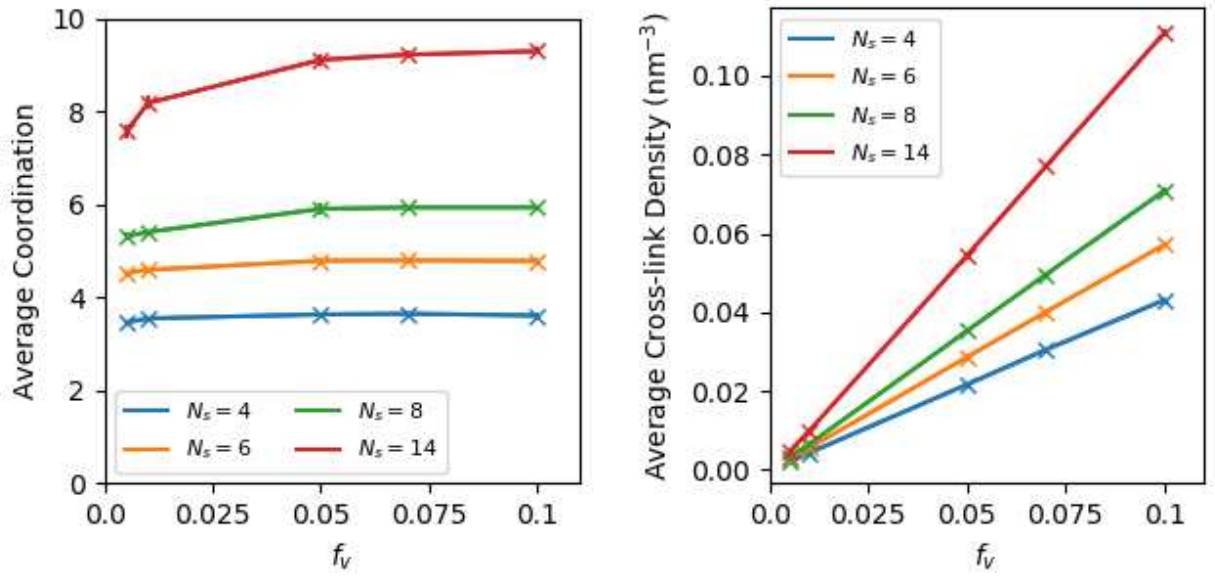

(a) (b)

Figure 4: The extrapolated value defining the expected final state of the network, and calculated through fitting Eq. 2 to the relevant data for $R = 1$nm simulations. a) Cross-link coordination number, C_{cl}. b) Spatial cross-link density, n_{cl}.

distributions of these multiple bonds and their radial distribution functions are shown in the Supplementary Information). As the proteins are given three-dimensional structure from their soft-core potentials, and the intrinsic stiffness k_s is kept constant between the two sets of simulations, then we find that it is easier to volumetrically 'deform' smaller proteins than larger ones. Hence, whilst atomistic bonding geometries are not taken into account in these coarse-grained simulations, we nevertheless see that for sufficiently soft proteins, higher levels of cross-linking may be expected.

As such, the overall cross-link density shown in Figure 4b is higher both because the proteins are smaller, leading to a higher density of cross-linking sites in space anyway, but also because the protein is sufficiently soft at this scale as to deform and allow multiple bonds to form. Thus we see the same qualitative pattern in both $R = 1$nm and $R = 2.5$nm simulations for the cross-link density, but a significantly higher absolute value in all cases when $R = 1$nm.

The combination of these insights implies that increasing the volume fraction of a protein hydrogel does not alter the local network structure, but simply provides additional protein material to fill in the gaps in the network. This is comparable to the wealth of work on the reinforcement of gels using so-called 'fillers', in which large particles are added to fill space in the gel matrix leading to reinforcement of the gel and an increase mechanical strength.[53,54] Nevertheless, whilst an increase in either N_s or f_v will increase the overall spatial cross-link density, increasing f_v homogeneously spreads these new cross-links through space together with new proteins, whereas increasing N_s must necessarily localise the new cross-links on the same number of proteins. This has ramifications for the way in which the protein network subsequently responds to both swelling and externally applied forces,[55] and more locally, which proteins in the network will unfold. However, questions involving protein folding require additional models to be developed and so will not be addressed in this work.

Network Structure

From this point forward we will be considering the final frames of the simulations for structural analysis, not extrapolations. Thus it is important to keep in mind the percolation analysis detailed in Supplementary Information, in that whilst we have indications of system spanning clusters in each of our analysed systems, there are some simulations in which all proteins are not connected into a single cluster.

The fractal dimension increases with volume fraction, but decreases with the number of available cross-link sites

In the previous sections we calculated average single protein properties over the network domain. We now begin to analyse our networks as single objects by calculating their volumetric fractal dimensions. The fractal dimension is a measure of how the volume of network structure fills the physical space in which it exists.[56] More colloquially, it is a measure of how 'branched' the structure is. Figure 5 shows the fractal dimensions of the final states of

each simulation considered, calculated using the box counting algorithm as detailed in the Supplementary Information. Whilst these fractal dimensions are strictly only valid up to the maximum box size of each simulation, recent simulations of colloidal gels analysed using the structure factor also yield similar fractal dimensions specifically at a volume fraction of ~ 0.05.[57] Additionally, whilst they are not percolated, we present analysis of the $f_v = 0.005$ and $f_v = 0.01$ simulation sets, as the fractal properties are of interest.

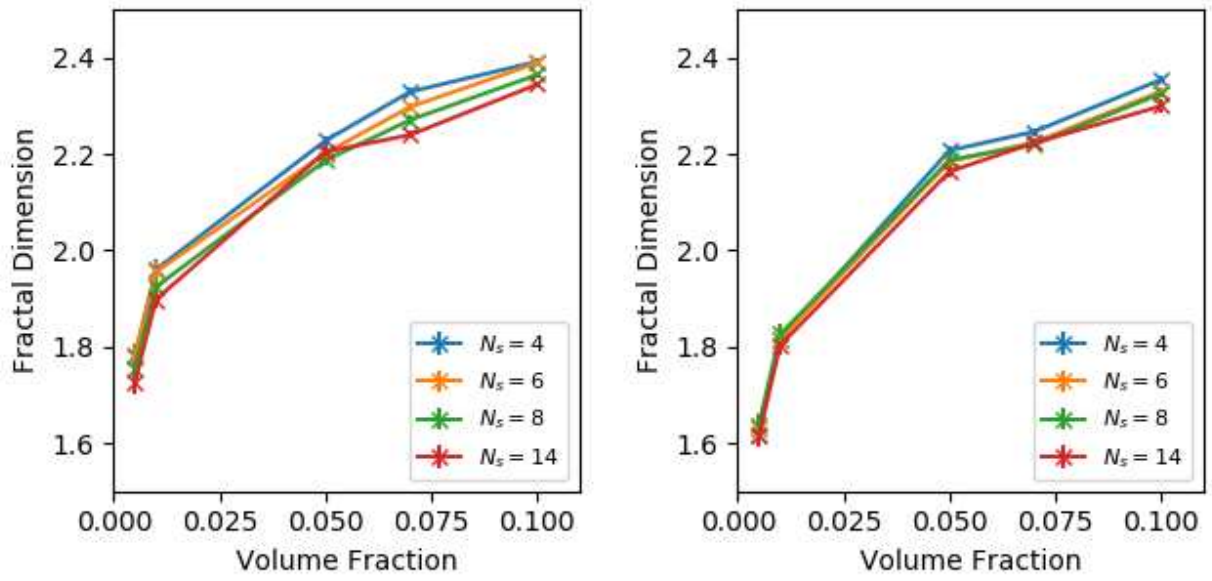

Figure 5: The fractal dimensions of the final state of each simulation, for a range of volume fractions of cross-link site topologies, calculated via the box counting algorithm detailed in Supplementary Information. **a)** $R = 1$nm. **b)** $R = 2.5$nm

We immediately see from Figure 5 that the volume fraction appears to be the dominant factor in determining the fractal dimension. Although the fractal dimension is a measure of how space is filled at different length scales, it is not necessarily true that it must increase with volume fraction as packing effects must also be considered. Nevertheless, in light of our previous observation that increasing f_v does not alter the local cross-link coordination i.e. the packing behaviour, then we indeed observe that as f_v increases, so too does D_f. However, we see that this increase may be tending towards a plateau which seems likely

to occur at a relatively low volume fraction, especially with respect to the glass transition volume fraction.[58] This shows that the formation of covalent cross-links, highly localised and deep energy wells,[44] prevents the non-specific geometric minimisations one would expect in comparable colloidal systems.[59,60]

We also note that as we increase the volume fraction we cross over from a value of $1 < D_f < 2$, representing a fibrillar structure, to one of $2 < D_f < 3$, representing a rough surface-like structure, at some point between $f_v = 0.01$ and $f_v = 0.05$. We did not achieve system-wide percolation for the $f_v \leq 0.01$ simulations, and so it may be that these two characteristics are related, as these measured surface-like fractal structures could be envisaged as encapsulating the volume of the system. However, we merely wish to emphasise that all of our percolated systems have $D_f > 2$.

The effect of variations in N_s on D_f is smaller in magnitude over the entire range of f_v considered, but has the opposite effect to a change in f_v. In other words, increases in N_s result in a slightly lower value of D_f, whereas an increase in f_v results in a slightly higher value of D_f. This shows that alterations in the local cross-link topology of each protein alters the structure at the network level by making it slightly more branched, as a higher value of N_s implies that there exist more potential paths between any two proteins in the network. This has implications in how force is distributed around the network and will potentially affect which, or even whether, proteins unfold upon swelling.[9,55]

Finally, we note that the $R = 2.5$nm simulations have a slightly lower value of D_f than their $R = 1$nm counterparts, but retain the same qualitative trends. We believe that this is due to the fact that the $R = 1$nm systems are able to form multiple bonds (see Supplementary Information), thus making them pack more efficiently as the proteins 'deform' i.e. overlap to accommodate multiple bonds.

Pore sizes decrease with volume fraction and the number of available binding sites

To observe the negative space surrounding the network, we calculate the pore size distribution throughout the network as defined by the maximal-ball algorithm.[61,62] This algorithm identifies pores by discretising space into a set of voxels (tessellating cubes) and calculating the minimum distance from the center of each of these voxels to the nearest protein surface. Following this, the pores are placed in a connected hierarchy where the locally largest of these are isolated as representative of the empty space within the structure (see Figure 6). Figure 7 shows the probability distributions of pore radii for each of the $R = 1$nm simulations, overlayed the inter-quartile range (IQR) and median. Each probability distribution was obtained from the combined set of pores from each of the three repeats. Due to the computational complexity of this problem, results are shown only for the highest three volume fractions, representing the percolated systems, using a voxel of length $4R$ to discretise space.

We see that all length scales associated with the pores (IQR, median and maximum) show at least a slight tendency to decrease with volume fraction, with the exception of the smallest pore measurable which remains constant at approximately $2R$. However, this minimum value is likely be constrained by our choice of voxel size. The maximum pore size also represents a single extreme data point, and is thus less predictable. It is clear that the IQR decreases most sharply with volume fraction, which corresponds to the contraction of the distribution of pore sizes around the median value. The median itself reduces only slightly with volume fraction, which may indicate that the median is more dependent upon the size of the subunits themselves, rather than their overall population. This has a parallel with our previous observations in Figure 3 of the volume fraction increasing the overall cross-link density whilst keeping the local cross-link coordination approximately constant. Thus, we can consider the reduction in the IQR with volume fraction to again be due to space being filled by the additional protein subunits.

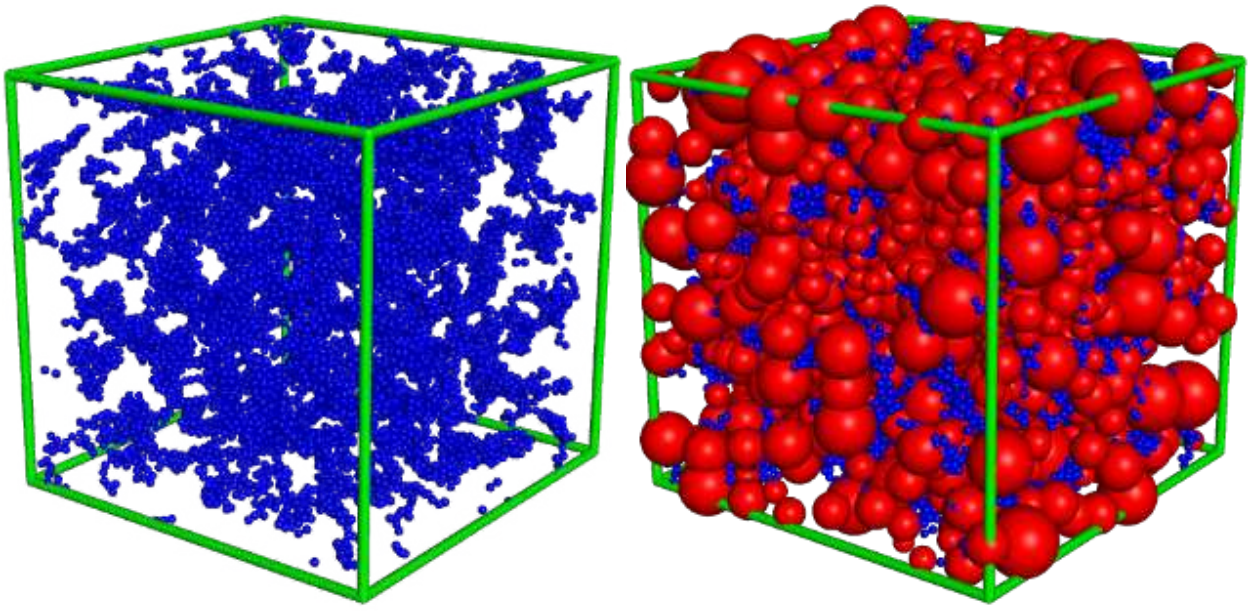

(a) (b)

Figure 6: Visualisations of the pores calculated by the maxima-ball algorithm for one of the $R = 2.5$nm, $f_v = 0.05$, $N_s = 8$ simulations. **a)** The network calculated by BioNet, with protein spheres shown in blue. **b)** Pores, show in red, overlaying the same network. They can exist 'outside' the simulation box slightly as periodic boundary conditions are taken into account.

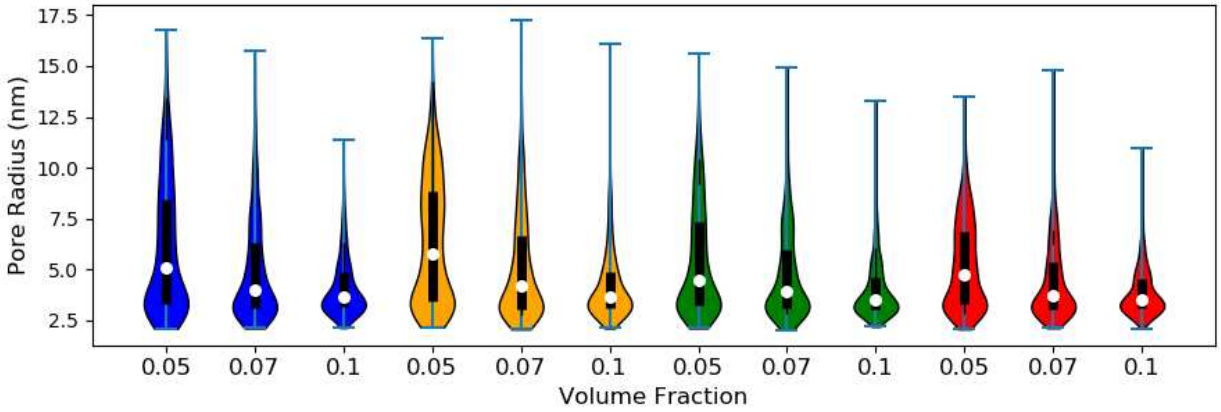

Figure 7: A 'violin' plot showing the normalised probability distributions of pore radii, calculated via performing the classical maximal ball algorithm on the final state of each of the $R = 1$nm simulations, for a range of volume fractions f_v and cross-link site topologies N_s. Each N_s is represented by a different colour. Blue: $N_s = 4$, Orange: $N_s = 6$, Green: $N_s = 8$, Red: $N_s = 14$

Of most interest is how the IQR, and indeed all of these size parameters, are dependent on number of binding sites N_s. We see that an increase in N_s, for any given value of f_v and with the strange exception of $N_s = 4$, reduces the value of each size parameter. With reference to our fractal dimension calculations, we hypothesise that an increase in N_s causes a more branched structure to form. For the same volume fraction, those additional branches must 'cut through' pores that would exist at lower values of N_s, and hence reduce both the expected size and, by eliminating larger pores, the IQR.

As a final note, the $R = 2.5$nm simulations showed similar trends in the parameters f_v and N_s, but generated larger pores. This data is provided as Supplementary Information.

Discussion

Throughout this simulation study we have analysed a range of emergent structural complexity of protein hydrogel networks as a function of various experimentally controllable parameters. Given the timescales involved, we hypothesise that these networks represent the state of the protein hydrogel network prior to the onset of swelling and subsequent protein unfolding. We have found that at the individual protein level, the volume fraction f_v has only a small effect on the cross-link coordination number C_{cl}. Instead, even though saturation is never achieved, it is the binding site topology of each protein subunit (represented by N_s) which dominates the local cross-linking. This feature scales up to the network level, where a higher value of N_s, and thus a higher C_{cl}, leads to a lower value of the fractal dimension D_f. We can infer from this that specific design of the individual protein subunits can lead to a more (or less) branched structure.

We have also seen that whilst not changing the local cross-link coordination, increasing the volume fraction offsets a lowering of the fractal dimension simply by filling in the empty space within the network. This comes with an associated increase in the overall spatial cross-link density n_{cl}, as each new protein can and will from additional cross-links, but also

with a decrease in the expected pore size and a reduction in the range of pore sizes. As an increase in N_s also slightly reduces the expected pore size, we can therefore infer that an increased cross-link density must be traded off with a decrease in pore sizes. This behaviour is also observed in standard biopolymer hydrogels[7] where it can be linked to stiffness,[51] and is likely a general phenomenon.

Finally, the effect of increasing the protein radius R is a reduction in the overall spatial cross-link density whilst retaining the lack of dependence on the volume fraction for the cross-link coordination number. In the limit of relatively small or soft proteins we may also observe multiple cross-links forming between pairs of proteins but in general, by increasing the size of a protein (whilst keeping the same volume fraction), we are effectively replacing covalent cross-links with the intra-protein bonds between folded amino acid chains. As a small side note, it has been known for the last decade in the field of colloidal glasses that the effect of soft particles allows for novel types of mechanical behaviour to emerge at high volume fractions, close to the glass transition.[63–65] For example, where a hard colloid would not be able to continue to diffuse past its closely packed neighbours, a soft colloid could physically deform in order to continue to diffuse, albeit over much longer time scales, in a phenomenon is known as cage-breaking.[58,65] Recent work on colloidal gels suggests that elastic effect may begin to emerge at volume fractions much lower than the system-wide glass transition volume fraction due to the effects of locally packed clusters.[66] Here, it is interesting to observe that microscopic fluctuations in the shape of nanoscale objects such as globular proteins may also lead to deformation significant enough to cause non-equilibrium effects, such as kinetic formation of new cross-links.

Various hypotheses may be drawn from these observations. First, the differences in network topology coupled to the structure of individual protein subunits implies that we can alter how force is distributed around the network simply by altering cross-link topology of the protein subunit. In contrast to the examples given in the seminal work of Wu *et al*,[26] in which multiple types of protein building block with different intrinsic properties are given

specific mechanical roles within the network, roles such as the 'load-bearing modules', our simulations instead suggest that the network structure itself may be altered whilst retaining the protein building block (albeit with a slightly different residue structure to alter the binding site topology). Thus the role of load-bearing module in our systems would not be decided by the intrinsic properties of the protein subunit, but instead by its location within the network hierarchy. If we assume equipartition of thermal energy within each cross-link, using our value of k_{cl}, we find that the expected elastic force due to thermal fluctuations is ~ 40pN *per cross-link*, showing that the stresses these proteins are experiencing even in their most relaxed state is relatively high, and even on the verge of unfolding already.[35,67] Figure 8a shows the distribution of these forces for one of our simulations, coloured by the instantaneous forces they are experiencing, showing the complexity of force distribution throughout these networks. And indeed, Figure 8b shows that the instantaneous force experienced by each protein is approximately proportional to the coordination number. However, the proteins at higher coordination numbers are clearly more deeply packed into the clusters, and so there may be no space for them to unfold into. Entropy, and packing, are also factors. For hydrogels whose viscoelastic response is mediated by protein unfolding,[27,29,30,49] control over how this force and the forces of swelling and external stresses are distributed throughout the system is therefore vital for rational design.[55]

Interestingly, Hughes *et al.* experimentally measure higher fractal dimensions than we do for the clusters present in their globular MBP hydrogels, which are best represented by our $R = 2.5$nm, $f_v = 0.1$, $N_s = 14$ simulation set. Using box counting, we measure $D_f = 2.30 \pm 0.02$ whereas using SANS measurements they measure $D_f = 2.41 \pm 0.05$, and using SAXS 2.60 ± 0.03. Given that the diffusion-limited connectivity will likely be conserved upon unfolding, as proteins will unfold before the cross-links will break, this discrepancy strongly suggests that the subsequent protein unfolding present in their gels causes denser clusters to form (i.e. locally increases f_v). We intend to explicitly model protein unfolding in our future work, using these simulations as a starting point.

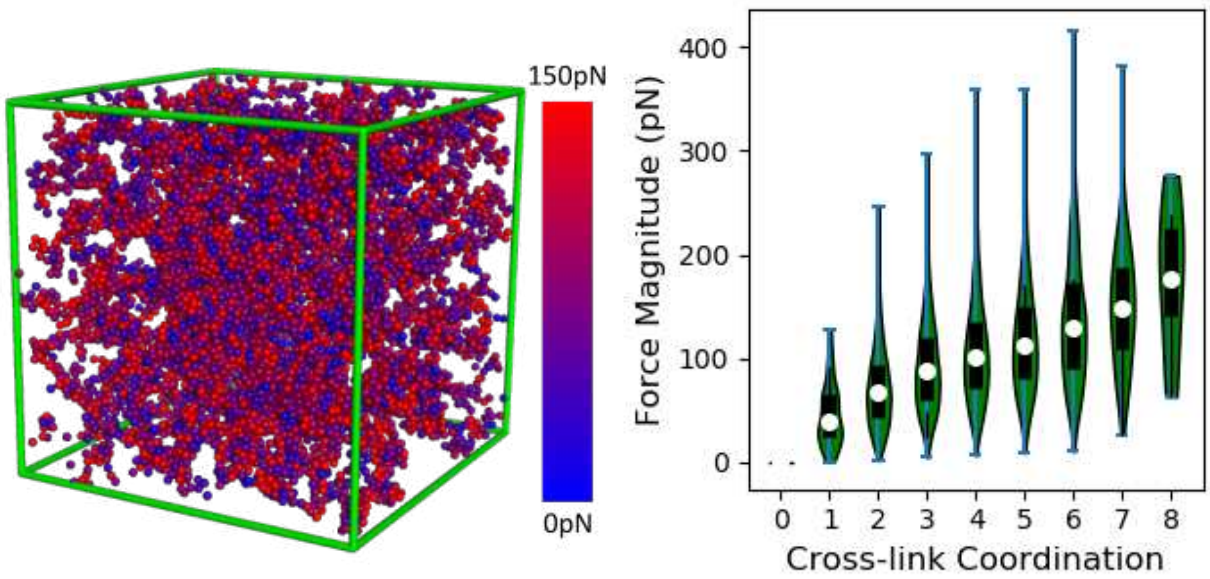

(a) (b)

Figure 8: The distribution of force around the network formed with proteins of radius $R = 2.5$nm, $N_s = 8$ cross-linking sites and a volume fraction $f_v = 0.07$. **a)** The network itself, with proteins coloured to represent the instantaneous conservative force (magnitude) each is experiencing. The maximum force, 150pN, represents the average unfolding force calculated from the proteins listed by Brockwell *et al.* ,[67] and any protein above this force is coloured at this level. **b)** The actual distributions of force as a function of coordination number, plotted as a 'violin' plot.

We hypothesise that an increase in the overall cross-link density generated by an increase in f_v will provide new, homogeneously distributed load-bearing modules to compensate for the additional energy density added when more cross-links form. On the other hand, if we instead increase N_s then those new cross-links must be localised to the existing load-bearing modules, further increasing the stress. Thus we might expect the internal stresses of each protein induced by swelling to be greater for large N_s than for large f_v. Such a trend can perhaps already be inferred from the recent work of Nguyen *et al.* , who in a similar vein observed the rheological behaviour of patchy colloidal gels as a function of the number of patches per colloid interaction potential of each patch.[57] They found that the measured low frequency storage modulus significantly increased at both higher interaction potentials and with more patches on each colloid. The limiting case of their interaction potentials correspond to the subunits used in our simulations, with unbreakable covalent bonds and relatively stiff proteins. How these affect the resultant elasticities for protein hydrogels, though, will likely depend upon the unfolding kinetics of the individual proteins.

Aside from the elastic response, our analysis of the pore size distributions as a function of volume fraction suggests that after swelling, or even on the application of external forces where the effective volume fraction will decrease, we may be able to increase the effective diffusion constant of our material by opening up new pathways for transmission i.e. providing more space for diffusion to occur. For objects on the order of the pores themselves, such as small nanobubbles,[68] this may enable a transformation between porous and non-porous states. Finally, because the volume fraction alters how much space is filled, it also directly affects cluster diffusion and first-pass times. It is well known that diffusion-limited aggregation leads to a lower fractal dimension than reaction-limited aggregation does,[69] and so from this point of view what we are seeing at higher volume fractions is our systems moving closer to a reaction-limited aggregation regime by reducing the relative diffusion times between intermediate clusters. However, as our reaction rate was set to be infinite, we could never truly enter the reaction-limited regime and hence, as can be seen in Figure 5, our fractal

dimensions and associated pore sizes eventually plateau. If we wish to surpass this fractal dimension limit, and create denser gels, a significant reduction in the reaction rate may be required to enter the reaction limited aggregation regime. As with biopolymer hydrogels, control over the reaction kinetics of protein hydrogels is a further parameter to be investigated. Additional work, both experimental and computational, is required to investigate these structural hypotheses.

To conclude, the simulations we have performed here and their resultant structures represent a potential starting point from which hydrodynamic swelling and protein unfolding can begin. From this point, it is clear that insight from the colloidal gel community will be vital moving forward. Whilst much work in this field occurs at 'intermediate' volume fractions beyond the protein solubility limit,[70] more recent work is concerned with lower volume fractions.[27,57,66] With an initial protein structure of choice, the radius of which will likely determine the average pore size, variations in the binding site topology and volume fraction allows us to tune our overall cross-link density (at the cost of pore size variance), cross-link coordination and fractal dimension. As the covalent cross-links are unlikely to break even upon swelling,[71] the structures observed here will potentially dominate the resultant topological structure of the network, and limit the subsequent structural rearrangements that can occur. For example, the higher the initial cross-link densities measured here, the shorter the lengths of amino acid chain would be upon protein unfolding and hence, the subsequent elastic response of the gel will likely have more of an enthalpic component than an entropic one. Whilst further simulations will be performed to encompass these effects, we hope that these mesoscopic structures provide new clarity on the hierarchical structural evolution of these fascinating biological materials.

Acknowledgement

We gratefully acknowledge funding from the Engineering and Physical Sciences Research

Council with grant EP/P02288X/1. The authors thank our colleague Kalila Cook for useful discussions on rate-limited and diffusion-limited aggregation. We also thank Dr David Head, who kindly provided us with a maximal-ball algorithm for reference. Much of this work was undertaken on ARC3, part of the high performance computing facilities at the University of Leeds, UK.

Supporting Information Available

A listing of the contents of each file supplied as Supporting Information should be included. For instructions on what should be included in the Supporting Information as well as how to prepare this material for publications, refer to the journal's Instructions for Authors.

The following files are available free of charge.

- Supplementary Information: .pdf containing non-vital information with regards to the core results.
- SimulationMovies: A (non-exhaustive) set of .mp4 files showing representative simulations.
    1. "Sites08_Radius1_Rate_VolFrac0.005.mp4" - A simulation with $N_S = 8$ cross-link sites per protein, sphere radius $R = 1$nm, and volume fraction $f_v = 0.005$
    2. "Sites08_Radius1_Rate_VolFrac0.05.mp4" - A simulation with $N_S = 8$ cross-link sites per protein, sphere radius $R = 1$nm, and volume fraction $f_v = 0.05$
    3. "Sites08_Radius1_Rate_VolFrac0.1.mp4" - A simulation with $N_S = 8$ cross-link sites per protein, sphere radius $R = 1$nm, and volume fraction $f_v = 0.1$
    4. "Sites08_Radius2.5_Rate_VolFrac0.005.mp4" - A simulation with $N_S = 8$ cross-link sites per protein, sphere radius $R = 2.5$nm, and volume fraction $f_v = 0.005$
    5. "Sites08_Radius2.5_Rate_VolFrac0.05.mp4" - A simulation with $N_S = 8$ cross-link sites per protein, sphere radius $R = 2.5$nm, and volume fraction $f_v = 0.05$

6. "Sites08_Radius2.5_Rate_VolFrac0.1.mp4" - A simulation with $N_S = 8$ cross-link sites per protein, sphere radius $R = 2.5$nm, and volume fraction $f_v = 0.1$

References

(1) Li, Y.; Xue, B.; Cao, Y. Synthetic Protein Hydrogels. *ACS Macro Letters* **2020**, *9*, 512–524.

(2) Fan, H.; Gong, J. P. Fabrication of Bioinspired Hydrogels: Challenges and Opportunities. *Macromolecules* **2020**, *53*, 2769–2782.

(3) Zhang, Y. S.; Khademhosseini, A. Advances in engineering hydrogels. *Science* **2017**, *356*.

(4) Vernerey, F. J.; Bryant, S. The role of percolation in hydrogel-based tissue engineering and bioprinting. *Current Opinion in Biomedical Engineering* **2020**, *15*, 68–74.

(5) Mondal, S.; Das, S.; Nandi, A. K. A Review on Recent Advances in Polymer and Peptide Hydrogels. *Soft Matter* **2020**, *16*, 1404–1454.

(6) Flory, P. J.; Rehner, J. Statistical mechanics of cross-linked polymer networks I. Rubberlike elasticity. *The Journal of Chemical Physics* **1943**, *11*, 512–520.

(7) Flory, P. J.; Rehner, J. Statistical mechanics of cross-linked polymer networks II. Swelling. *The Journal of Chemical Physics* **1943**, *11*, 521–526.

(8) Shmilovich, K.; Popa, I. Modeling Protein-Based Hydrogels under Force. *Physical Review Letters* **2018**, *121*, 168101.

(9) Khoury, L. R.; Popa, I. Chemical unfolding of protein domains induces shape change in programmed protein hydrogels. *Nature Communications* **2019**, *10*, 1–9.

(10) Lv, S.; Dudek, D. M.; Cao, Y.; Balamurali, M. M.; Gosline, J.; Li, H. Designed biomaterials to mimic the mechanical properties of muscles. *Nature* **2010**, *465*, 69–73.

(11) Billiet, T.; Vandenhaute, M.; Schelfhout, J.; Van Vlierberghe, S.; Dubruel, P. A review of trends and limitations in hydrogel-rapid prototyping for tissue engineering. *Biomaterials* **2012**, *33*, 6020–6041.

(12) Hoffman, A. S. Hydrogels for biomedical applications. *Advanced Drug Delivery Reviews* **2012**, *64*, 18–23.

(13) Gyles, D. A.; Castro, L. D.; Silva, J. O. C.; Ribeiro-Costa, R. M. A review of the designs and prominent biomedical advances of natural and synthetic hydrogel formulations. *European Polymer Journal* **2017**, *88*, 373–392.

(14) Asadi, N.; Alizadeh, E.; Salehi, R.; Khalandi, B.; Davaran, S.; Akbarzadeh, A. Nanocomposite hydrogels for cartilage tissue engineering: a review. *Artificial Cells, Nanomedicine and Biotechnology* **2018**, *46*, 465–471.

(15) Sackett, S. D.; Tremmel, D. M.; Ma, F.; Feeney, A. K.; Maguire, R. M.; Brown, M. E.; Zhou, Y.; Li, X.; O'Brien, C.; Li, L.; Burlingham, W. J.; Odorico, J. S. Extracellular matrix scaffold and hydrogel derived from decellularized and delipidized human pancreas. *Scientific Reports* **2018**, *8*, 1–16.

(16) Sun, Y.; Nan, D.; Jin, H.; Qu, X. Recent advances of injectable hydrogels for drug delivery and tissue engineering applications. *Polymer Testing* **2020**, *81*, 106283.

(17) Lee, J. H. Injectable hydrogels delivering therapeutic agents for disease treatment and tissue engineering. *Biomaterials Research* **2018**, *22*, 1–14.

(18) Zhang, X.; Jiang, S.; Yan, T.; Fan, X.; Li, F.; Yang, X.; Ren, B.; Xu, J.; Liu, J. Injectable and fast self-healing protein hydrogels. *Soft Matter* **2019**, *15*, 7583–7589.

(19) Sun, G.; Zhang, X.; Shen, Y. I.; Sebastian, R.; Dickinson, L. E.; Fox-Talbot, K.; Reinblatt, M.; Steenbergen, C.; Harmon, J. W.; Gerecht, S. Dextran hydrogel scaffolds enhance angiogenic responses and promote complete skin regeneration during burn wound healing. *Proceedings of the National Academy of Sciences of the United States of America* **2011**, *108*, 20976–20981.

(20) Wang, J.; Hao, S.; Luo, T.; Cheng, Z.; Li, W.; Gao, F.; Guo, T.; Gong, Y.; Wang, B. Feather keratin hydrogel for wound repair: Preparation, healing effect and biocompatibility evaluation. *Colloids and Surfaces B: Biointerfaces* **2017**, *149*, 341–350.

(21) Blacklow, S. O.; Li, J.; Freedman, B. R.; Zeidi, M.; Chen, C.; Mooney, D. J. Bioinspired mechanically active adhesive dressings to accelerate wound closure. *Science Advances* **2019**, *5*, 1–10.

(22) Hughes, M. L.; Dougan, L. The physics of pulling polyproteins: A review of single molecule force spectroscopy using the AFM to study protein unfolding. *Reports on Progress in Physics* **2016**, *79*, 076601.

(23) Hanson, B. S.; Head, D.; Dougan, L. The hierarchical emergence of worm-like chain behaviour from globular domain polymer chains. *Soft Matter* **2019**, *15*, 8778–8789.

(24) Hill, L. K.; Meleties, M.; Katyal, P.; Xie, X.; Delgado-Fukushima, E.; Jihad, T.; Liu, C. F.; O'Neill, S.; Tu, R. S.; Renfrew, P. D.; Bonneau, R.; Wadghiri, Y. Z.; Montclare, J. K. Thermoresponsive Protein-Engineered Coiled-Coil Hydrogel for Sustained Small Molecule Release. *Biomacromolecules* **2019**, *20*, 3340–3351.

(25) Fu, L.; Haage, A.; Kong, N.; Tanentzapf, G.; Li, H. Dynamic protein hydrogels with reversibly tunable stiffness regulate human lung fibroblast spreading reversibly. *Chemical Communications* **2019**, *55*, 5235–5238.

(26) Wu, J.; Li, P.; Dong, C.; Jiang, H.; Xue, B.; Gao, X.; Qin, M.; Wang, W.; Bin Chen,;

Cao, Y. Rationally designed synthetic protein hydrogels with predictable mechanical properties. *Nature Communications* **2018**, *9*, 1–11.

(27) Hughes, M. D. G.; Cussons, S.; Mahmoudi, N.; Brockwell, D. J.; Dougan, L. Single-molecule protein stabilisation translates to macromolecular mechanics of protein networks. *Soft Matter* **2020**, In press.

(28) Da Silva, M. A.; Lenton, S.; Hughes, M.; Brockwell, D. J.; Dougan, L. Assessing the Potential of Folded Globular Polyproteins As Hydrogel Building Blocks. *Biomacromolecules* **2017**, *18*, 636–646.

(29) Khoury, L. R.; Nowitzke, J.; Shmilovich, K.; Popa, I. Study of Biomechanical Properties of Protein-Based Hydrogels Using Force-Clamp Rheometry. *Macromolecules* **2018**, *51*, 1441–1452.

(30) Fang, J.; Mehlich, A.; Koga, N.; Huang, J.; Koga, R.; Gao, X.; Hu, C.; Jin, C.; Rief, M.; Kast, J.; Baker, D.; Li, H. Forced protein unfolding leads to highly elastic and tough protein hydrogels. *Nature Communications* **2013**, *4*, 1–10.

(31) Grad, E. M.; Tunn, I.; Voerman, D.; Léon, A. S. D.; Hammink, R.; Blank, K. Influence of Network Topology on the Viscoelastic Properties of Dynamically Crosslinked Hydrogels. *ChemRxiv* **2020**, http://doi.org/10.26434/chemrxiv.11763792.v1.

(32) Hennink, W. E.; van Nostrum, C. F. Novel crosslinking methods to design hydrogels. *Advanced Drug Delivery Reviews* **2012**, *64*, 223–236.

(33) Hu, W.; Wang, Z.; Xiao, Y.; Zhang, S.; Wang, J. Advances in crosslinking strategies of biomedical hydrogels. *Biomaterials Science* **2019**, *7*, 843–855.

(34) Studier, F. W. Protein production by auto-induction in high density shaking cultures. *Protein expression and purification* **2005**, *41*, 207–234.

(35) Hoffmann, T.; Dougan, L. Single molecule force spectroscopy using polyproteins. *Chemical Society Reviews* **2012**, *41*, 4781–4796.

(36) Hoffmann, T.; Tych, K. M.; Hughes, M. L.; Brockwell, D. J.; Dougan, L. Towards design principles for determining the mechanical stability of proteins. *Physical Chemistry Chemical Physics* **2013**, *15*, 15767–15780.

(37) Bjork, J. W.; Johnson, S. L.; Tranquillo, R. T. Ruthenium-catalyzed photo cross-linking of fibrin-based engineered tissue. *Biomaterials* **2011**, *32*, 2479–2488.

(38) Fancy, D. A.; Denison, C.; Kim, K.; Xie, Y.; Holdeman, T.; Amini, F.; Kodadek, T. Scope, limitations and mechanistic aspects of the photo-induced cross-linking of proteins by water-soluble metal complexes. *Chemistry and Biology* **2000**, *7*, 697–708.

(39) Kyburz, K. A.; Anseth, K. S. Synthetic Mimics of the Extracellular Matrix: How Simple is Complex Enough? *Annals of Biomedical Engineering* **2015**, *43*, 489–500.

(40) Caccavo, D.; Lamberti, G. PoroViscoElastic model to describe hydrogels' behavior. *Materials Science and Engineering C* **2017**, *76*, 102–113.

(41) Caccavo, D.; Lamberti, G.; Barba, A. A. Mechanics and drug release from poroviscoelastic hydrogels: Experiments and modeling. *European Journal of Pharmaceutics and Biopharmaceutics* **2020**, *152*, 299–306.

(42) Brockwell, D. J.; Paci, E.; Zinober, R. C.; Beddard, G. S.; Olmsted, P. D.; Smith, D. A.; Perham, R. N.; Radford, S. E. Pulling geometry defines the mechanical resistance of a β-sheet protein. *Nature Structural Biology* **2003**, *10*, 731–737.

(43) Landau, L.; Lifshitz, E. *Fluid Mechanics: Course of Theoretical Physics Vol. 6*, 2nd ed.; Butterworth-Heinemann, 1987.

(44) Jorgensen, W. L.; Maxwell, D. S.; Tirado-Rives, J. Development and testing of the

OPLS all-atom force field on conformational energetics and properties of organic liquids. *Journal of the American Chemical Society* **1996**, *118*, 11225–11236.

(45) Witten, T. Diffusion-Limited Aggregation, a Kinetic Critical Phenomenon. *Physical Review Letters* **1981**, *47*, 1400–1403.

(46) Wang, H.; Shi, Y.; Wang, L.; Yang, Z. Recombinant proteins as cross-linkers for hydrogelations. *Chemical Society Reviews* **2013**, *42*, 891–901.

(47) Sun, W.; Duan, T.; Cao, Y.; Li, H. An Injectable Self-Healing Protein Hydrogel with Multiple Dissipation Modes and Tunable Dynamic Response. *Biomacromolecules* **2019**, *20*, 4199–4207.

(48) Tang, Z.; Chen, Q.; Chen, F.; Zhu, L.; Lu, S.; Ren, B.; Zhang, Y.; Yang, J.; Zheng, J. General Principle for Fabricating Natural Globular Protein-Based Double-Network Hydrogels with Integrated Highly Mechanical Properties and Surface Adhesion on Solid Surfaces. *Chemistry of Materials* **2019**, *31*, 179–189.

(49) Kong, N.; Peng, Q.; Li, H. Rationally designed dynamic protein hydrogels with reversibly tunable mechanical properties. *Advanced Functional Materials* **2014**, *24*, 7310–7317.

(50) Fischer, H.; Polikarpov, I.; Craievich, A. F. Average protein density is a molecular-weight-dependent function. *Protein Science* **2009**, *13*, 2825–2828.

(51) Broedersz, C. P.; Mackintosh, F. C. Modeling semiflexible polymer networks. *Reviews of Modern Physics* **2014**, *86*, 995–1036.

(52) Towey, J. A Structural Approach to Reveal the Croprotective Action of Glycerol. Ph.D. thesis, University of Leeds, 2013.

(53) Genovese, D. B. Shear rheology of hard-sphere, dispersed, and aggregated suspensions,

and filler-matrix composites. *Advances in Colloid and Interface Science* **2012**, *171-172*, 1–16.

(54) Ducloué, L.; Pitois, O.; Goyon, J.; Chateau, X.; Ovarlez, G. Coupling of elasticity to capillarity in soft aerated materials. *Soft Matter* **2014**, *10*, 5093–5098.

(55) Fan, Q.; Chen, B.; Cao, Y. Constitutive model reveals the defect-dependent viscoelasticity of protein hydrogels. *Journal of the Mechanics and Physics of Solids* **2019**, *125*, 653–665.

(56) Falconer, K. *Fractal geometry : mathematical foundations and applications*, 2nd ed.; Wiley, 1952.

(57) Nguyen, H. T.; Graham, A. L.; Koenig, P. H.; Gelb, L. D. Computer simulations of colloidal gels: How hindered particle rotation affects structure and rheology. *Soft Matter* **2019**, *16*, 256–269.

(58) Hunter, G. L.; Weeks, E. R. The physics of the colloidal glass transition. *Reports on Progress in Physics* **2012**, *75*, 066501.

(59) Wang, J.; Mbah, C. F.; Przybilla, T.; Zubiri, B. A.; Spiecker, E.; Engel, M.; Vogel, N. Magic number colloidal clusters as minimum free energy structures. *Nature Communications* **2018**, *9*, 1–10.

(60) Cersonsky, R. K.; Van Anders, G.; Dodd, P. M.; Glotzer, S. C. Relevance of packing to colloidal self-assembly. *Proceedings of the National Academy of Sciences of the United States of America* **2018**, *115*, 1439–1444.

(61) Arand, F.; Hesser, J. Accurate and efficient maximal ball algorithm for pore network extraction. *Computers and Geosciences* **2017**, *101*, 28–37.

(62) Silin, D.; Patzek, T. Pore space morphology analysis using maximal inscribed spheres. *Physica A: Statistical Mechanics and its Applications* **2006**, *371*, 336–360.

(63) Mattsson, J.; Wyss, H. M.; Fernandez-Nieves, A.; Miyazaki, K.; Hu, Z.; Reichman, D. R.; Weitz, D. A. Soft colloids make strong glasses. *Nature* **2009**, *462*, 83–86.

(64) Koumakis, N.; Pamvouxoglou, A.; Poulos, A. S.; Petekidis, G. Direct comparison of the rheology of model hard and soft particle glasses. *Soft Matter* **2012**, *8*, 4271–4284.

(65) Gnan, N.; Zaccarelli, E. The microscopic role of deformation in the dynamics of soft colloids. *Nature Physics* **2019**, *15*, 683–688.

(66) Whitaker, K. A.; Varga, Z.; Hsiao, L. C.; Solomon, M. J.; Swan, J. W.; Furst, E. M. Colloidal gel elasticity arises from the packing of locally glassy clusters. *Nature Communications* **2019**, *10*.

(67) Brockwell, D. J.; Beddard, G. S.; Paci, E.; West, D. K.; Olmsted, P. D.; Smith, D. A.; Radford, S. E. Mechanically unfolding the small, topologically simple protein L. *Biophysical Journal* **2005**, *89*, 506–519.

(68) Batchelor, D. V. B.; Abou-Saleh, R. H.; Coletta, P. L.; McLaughlan, J. R.; Peyman, S. A.; Evans, S. D. Nested Nanobubbles for Ultrasound-Triggered Drug Release. *ACS Applied Materials & Interfaces* **2020**, *12*, 29085–29093.

(69) Lin, M. Y.; Lindsayt, H. M.; Weitz, D. A.; Ballt, R. C.; Klein, R.; Meakinll, P. Universality in colloid aggregation. *Nature* **1989**, *339*, 360–362.

(70) Capellmann, R. F.; Valadez-Pérez, N. E.; Simon, B.; Egelhaaf, S. U.; Laurati, M.; Castañeda-Priego, R. Structure of colloidal gels at intermediate concentrations: the role of competing interactions. *Soft Matter* **2016**, *12*, 9303–9313.

(71) Grandbois, M.; Beyer, M.; Rief, M.; Clausen-Schaumann, H.; Gaub, H. E. How strong is a covalent bond. *Science* **1999**, *283*, 1727–1730.

(72) Jan, N. Large lattice random site percolation. *Physica A: Statistical Mechanics and its Applications* **1999**, *266*, 72–75.